Classification of Gases with Single FET-Based Gas Sensor Through Gate Voltage Sweeping and Machine Learning

Sarkar, Lisa; Paul, Soumen; Sett, Avik; Kumari, Ambika; Bhattacharyya, Tarun Kanti

DOI
10.1109/TED.2024.3486261

Publication date
2024

Document Version
Final published version

Published in
IEEE Transactions on Electron Devices

Classification of Gases With Single FET-Based Gas Sensor Through Gate Voltage Sweeping and Machine Learning

Lisa Sarkar, Soumen Paul, Avik Sett, Ambika Kumari, and Tarun Kanti Bhattacharyya

***Abstract*— Uncontrolled release of various harmful gases from automobiles and chemical industries demands accurate methods for gas classification and detection. In this context, this article proposes an effective method to classify and detect four gases—ammonia, formaldehyde, toluene, and acetone using a single field-effect transistor (FET)-based gas sensor. The gate voltage of the FET sensor played a pivotal role in this classification mechanism. L-ascorbic acid functionalized graphene oxide (GO) was used as the sensing material of the FET device. Initially, various features of the fabricated FET sensor (i.e., % of response, response time, and recovery time) were captured by varying the applied gate voltage. Furthermore, classification algorithms such as decision tree (DT), support vector machine (SVM), gradient boosting (GB), and random forest (RF) were trained to automatically predict the target gases. An accuracy of 73% was achieved for all three classifiers other than the SVM classifier. The use of machine learning algorithms was fruitful to accurately detect four gases at different gate voltages when any unknown one among the four was exposed to the single gate-tuned sensor. Moreover, it also saved the system's power consumption as a single sensor was behaving like several sensors.**

***Index Terms*— % of response, field-effect transistor (FET) sensor, gas classification/prediction, ML algorithms.**

I. Introduction

RECENT advancement of chemical and pharmaceutical industries gives rise to a serious problem of various toxic gas emissions in the environment. Ammonia, xylene, benzene, toluene, and formaldehyde are very common among those emitted gases. Inhalation of those harmful volatile organic compounds (VOC) and gases causes adverse health issues. So, automatic detection of pollutant gases and VOCs garnered significant interest in diverse fields ranging from personal safety to industrial application [1], [2], [3], [4], [5].

Received 18 October 2024; accepted 21 October 2024. Date of publication 26 November 2024; date of current version 31 December 2024. The review of this article was arranged by Editor M. M. Hussain. *(Lisa Sarkar and Soumen Paul contributed equally to the work.) (Corresponding author: Tarun Kanti Bhattacharyya.)*

Lisa Sarkar, Ambika Kumari, and Tarun Kanti Bhattacharyya are with the Department of Electronics and Electrical Communication Engineering, Indian Institute of Technology Kharagpur, Kharagpur 721302, India (e-mail: tkb@ece.iitkgp.ac.in).

Soumen Paul is with the Department of Computer Science and Engineering, Indian Institute of Technology Kharagpur, Kharagpur 721302, India.

Avik Sett is with the Department of Microelectronics, TU Delft, 2628 CD Delft, The Netherlands.

Digital Object Identifier 10.1109/TED.2024.3486261

There are several seminal papers reporting a variety of gas sensing mechanisms, such as resistive sensing, optical sensing, electrochemical sensing, and field-effect transistor (FET)-based sensing, to name a few. Among them, FET-based sensing mechanism has captivated the researcher owing to its ability of sensitivity amplification through optimization of gate electrostatics [6], [7], [8], [9]. FET sensors posses high sensitivity compared with other devices, as charge carrier mobility can be modulated by controlling the gate voltage [10]. Moreover, FET sensors have the inherent advantages of miniaturization, low cost, and low power consumption because of their CMOS compatibility. Numerous metal oxides (ZnO, In_2O_3, SnO_2, NiO, etc.) and 2-D materials (graphene, rGO, MoS_2) have extensively used for this purpose. Metal-oxide-based gas sensors are popular for their high response, large sensitivity, and simple operation [11], [12]. But they suffer from a serious bottleneck of high-temperature sensing which leads high power consumption. On the other hand, the 2-D material, reduced graphene oxide (rGO) is well-known for room temperature sensing. For preparation of rGO, graphene oxide (GO) is reduced by various reducing agents which in turn removes some oxygen containing groups and incorporates defect states. As a result, it increases active sites of rGO for gas adsorption and contributes toward improvement in selectivity to specific gases.

The most common method for detecting multiple gases is to use a sensor array containing multiple sensors. It would be really challenging and exciting if multiple gases can be detected with less number of sensors especially with a single sensor. This will also reduce the power consumption drastically. Very few reports were published on single-sensor-based gas discrimination methodology [13], [14], [15]. In one approach, temperature sweeping was used to discriminate multiple gases using a single chemiresistive sensor [13]. Another approach used transient feature analysis to enhance discrimination and classification of gases using a single resistive graphene sensor [14]. In another technique, discrimination was performed by analyzing the low-frequency noise of graphene in the presence of vapors of various chemicals [15]. In all the above-mentioned reports, experiments were performed with resistive gas sensor.

In this work, classification and accurate prediction of four gases is presented using a single FET sensor where L-ascorbic acid functionalized reduced GO (LA-rGO) was used as the sensing material. The FET sensor was exposed to different gases, and various features such as % of response, response

time, and recovery time of the sensor were captured by sweeping the gate voltage of the device and the concentration of gases. These three dependent features, along with two independent features, were used for the classification of gases. Consequently, different machine learning classification algorithms such as decision tree (DT), support vector machine (SVM), gradient boosting (GB), and random forest (RF) were trained, which automatically detected different gases. All three models, except the SVM, achieved similar detection performance for our data. The primary motivation for using machine learning algorithms in combination with the single FET sensor is twofold. First, it reduces the system's power consumption due to the elimination of multiple sensors. Along with that, it is also cost-effective as it is able to distinguish multiple gases with a single sensor and statistical analysis of the sensor's data.

II. Materials and Methods

A. Preparation of rGO

At first, GO was prepared from graphite powder using modified Hummer's method [16].

Furthermore, L-ascorbic acid was used to reduce the as-prepared GO solution. About 40 mg of L-Ascorbic acid was added to 40-mL GO solution (0.5 mg/mL) and kept in vigorous stirring for 1–2 h. The final solution was then kept in oven at 50 °C for 4.5 h to prepare rGO.

B. Fabrication of FET-Based Sensor

A heavily doped p-type Si wafer was used for FET sensor fabrication. In this work, silk film was used as gate dielectric instead of SiO_2 as silk possesses high dielectric constant and ultrasmooth surface [17]. For silk film preparation, at first silk solution was prepared from raw silk thread (Bombyx mori). Readily available raw silk was purchased from M/S Bombyx Mori Silks and Textiles, Srinagar, India. Then this raw silk was processed through a number of steps to prepare silk solution. The detail procedure was illustrated in our previous work [18]. In this work, 10 wt% silk–formic acid solution was prepared. This solution was then coated on Si substrate by spin-coating to form a 1-μm-thick silk film. While spin-coating, whole Si substrate was not covered by silk, and Si was exposed at two edges to get connection for gate terminal. Following that, Ti/Au layer of 20/200-nm thickness was deposited atop silk for source and drain formation. The channel length was kept fixed at 70 μm. The sensing material was dispersed in the channel by drop casting the material using a 20-μL micropipette. The schematic of the device is shown in Fig. 1.

C. Test and Measurement

The compositional analysis of rGO-LA was performed through FTIR (SHIMADZU IRtracer-100), XPS, and RAMAN (Witec alpha 300, 532-nm laser) studies. Morphological measurement was carried out through FESEM analysis. A semiconductor parameter analyzer (Agilent B1500A) was used for electrical characterization of the FET sensor, i.e., transfer and output characteristics. A customized setup from KYS Technologies was used to check the gas sensing mechanism of the fabricated sensor.

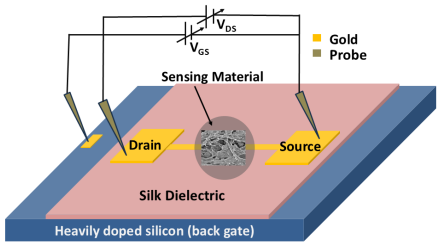

Fig. 1. Schematic of the FET-based sensor.

D. Machine Learning Methods for Gas Classification

The output characteristics of the sensor were exploited for automatic identification of gases. A list of classification algorithms was applied, which takes the sensor output characteristics as a feature set and classifies them into a predefined set of gases. We explored SVM, DT, GB, and RF algorithms for our gas classification task. Among them, the DT model predicts the target class by learning a set of decision rules inferred from the input data points. This approach needs a little data preparation and does not need data normalization. SVM is a powerful technique that works best for a smaller dataset. On the other hand, RF and GB methods work well for large and complex datasets. Moreover, GB is an ensemble method that builds models intelligently by giving more weights to those data samples that are hard to classify. Alternately, the RF classifier captures nonlinear relationships between input and target variables and is less prone to overfitting problems. We carefully selected these four machine learning models to understand the behavior of our data distribution.

III. Results and Discussion

A. Compositional and Morphological Analysis

FTIR analysis was carried out to check the composition of synthesized material. FTIR data are plotted in Fig. 2(a). GO exhibits a broad intense peak at 3424 cm^{-1} corresponding to hydroxyl (O–H) bond stretching [19]. GO also exhibits another prominent peak at 1630 cm^{-1} which represents the C=C bond. Few more peaks are also visible at 1220, 1052, and 872 cm^{-1} which are assigned to the stretching of C-OH bond, C–O–C bond, and epoxy ring [20], respectively. The FTIR spectrum of L-ascorbic acid reduced rGO is also shown in Fig. 2(a) where only two peaks located at 3424 and 1630 cm^{-1} are visible. The intensity of these two peaks reduces drastically.

Fig. 2(b) and (c) depicts the RAMAN spectra of GO and rGO. The D- and G-band of GO appears at 1354 and 1609 cm^{-1}, respectively. After reduction by L-ascorbic acid, the D-band shifts to 1363 cm^{-1}, whereas the G-band is at the same place 1609 cm^{-1}. The FWHM of the D- and G-band of both GO and rGO is computed by deconvoluting the Raman spectra. The ratio of I_D and I_G is found to be 0.94 and 1.56 for GO and rGO, respectively. The D-band basically represents sp^3 carbon or defects on the graphene sheet, and the G-band represents the in-plane vibration of sp^2 carbon atom. Various functional groups in GO were removed with the reduction while leaving some dangling bonds or defects.

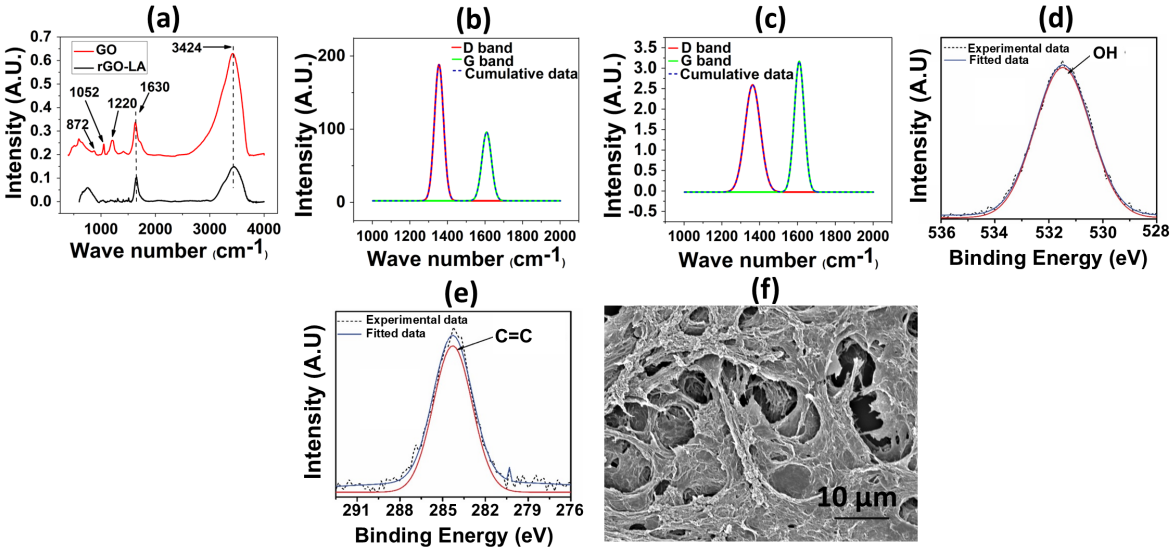

Fig. 2. (a) FTIR of GO and L-ascorbic acid reduced rGO. (b) RAMAN spectrum of GO. (c) RAMAN spectrum of rGO. (d) and (e) XPS high-resolution scan of rGO for oxygen and carbon. (f) FESEM image of L-ascorbic acid reduced rGO at 2.5 K magnification.

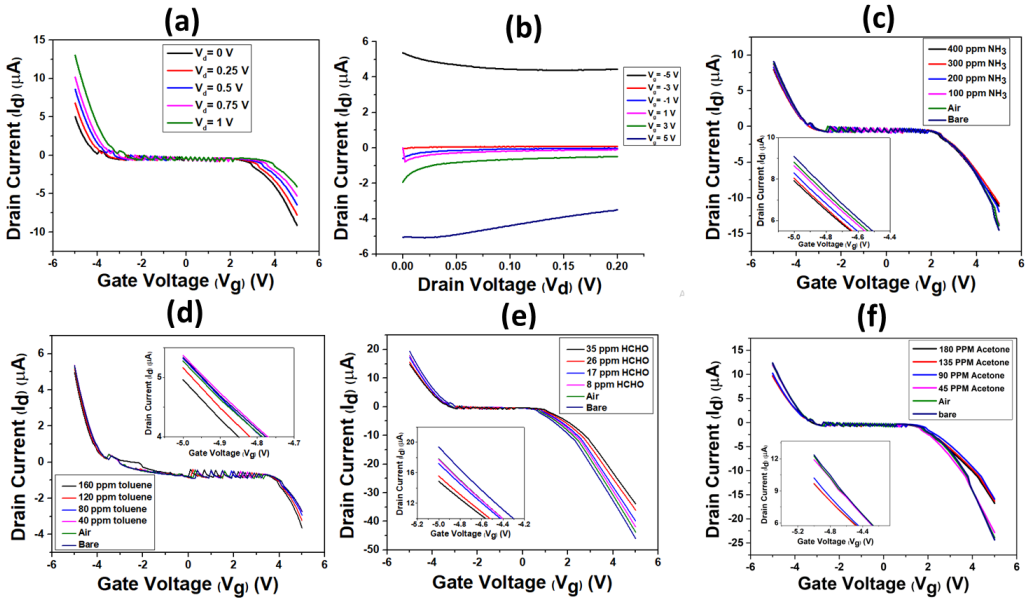

Fig. 3. FET sensor's (a) transfer characteristics for different V_d, (b) output characteristics for different V_g, and (c)–(f) transfer characteristics upon exposure to NH_3, toluene, HCHO, and acetone.

Those defects result in the formation of sp^3 clusters [21]. The higher I_D/I_G value indicates various defect states generated in rGO during functionalization which act as active sites for the physisorption of gases during sensing [22]. XPS analysis was also carried out to reaffirm the chemical composition of L-ascorbic acid reduced rGO. Fig. 2(d) and (e) shows the wide energy survey scan to identify the elements. The peak at 531.6 eV [Fig. 2(d)] represents the presence of OH bond and the peak at 284.6 eV [Fig. 2(d)] is attributed to C=C bond, respectively. The presence of these two bonds was also noted in the FTIR spectrum.

The FESEM micrograph of rGO was also captured for morphological analysis, and the FESEM image is shown in Fig. 2(f). A wrinkled sheet-like structure is observed. The presence of defects in rGO is the most probable reason for those wrinkles.

B. Electrical Measurements and Working Principle of FET Sensor

The transfer characteristics (I_d versus V_g) of the FET sensor is plotted in Fig. 3(a). It is seen that gate voltage V_g was varied from −5 to 5 V and the corresponding drain currents (I_d) were measured for different V_d (0–1 V). It is also noted that for a fixed drain-to-source voltage, I_d decreases with the increase in V_g. The drain current decreases due to depletion of a majority of carrier holes in the channel as rGO behaves like a p-type material. The same characteristic was followed for

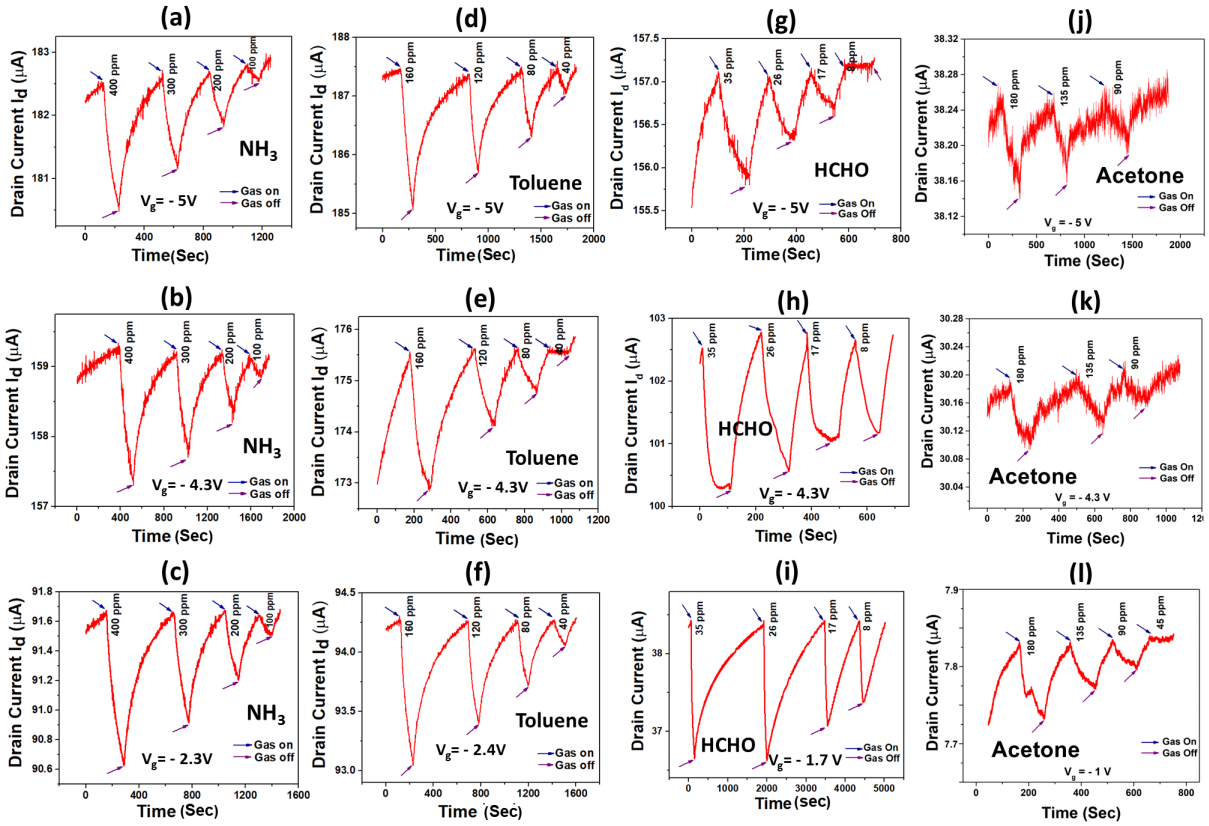

Fig. 4. Transient response (I_d versus time) of the sensor towards (a)–(c) ammonia gas exposure, (d)–(f) toluene gas exposure, (g)–(i) formaldehyde gas exposure, and (j)–(l) acetone gas exposure at different gate voltages and gas concentrations.

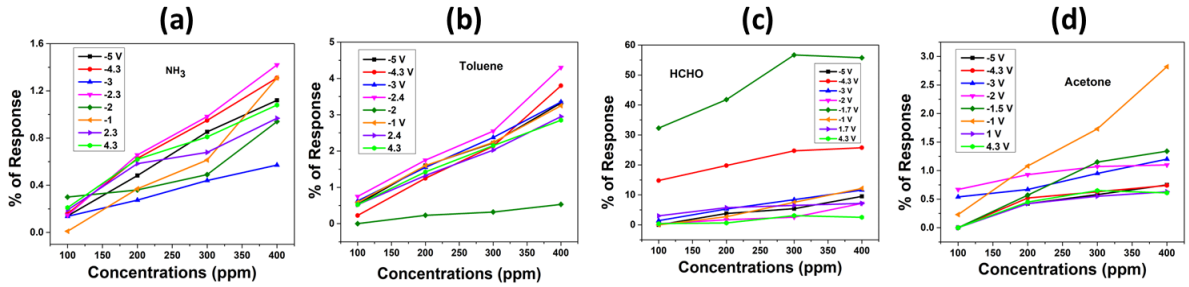

Fig. 5. Gate-voltage-dependent response of the sensor upon exposure of (a) NH_3, (b) toluene, (c) formaldehyde, and (d) acetone.

another drain voltages (V_d) while the drain current increases with V_d. The output characteristic of the fabricated FET sensor was also captured and is plotted in Fig. 3(b) for different V_g (-5 to 5 V). It is seen that the drain current increases linearly with the increase in V_d for $V_g = 5$ V, showing linear regime characteristics of FET. For $V_g = 3$ to -3 V, the drain current increases with V_d up to a certain V_d and then it saturates. The output characteristic also reveals the p-type nature of rGO as it is observed that the drain current decreases with the increase in gate voltage. The majority carrier hole decreases with the positive gate voltage. From transfer characteristics, the ON-current-to-OFF-current ratio of the FET device was calculated as 29 for a drain voltage of 1 V. The lower ON/OFF ratio is attributed to structural defects, residual oxygen groups in the rGO lattice, and adsorbed oxygen molecules from air. However, the structural defects give rise to a large number of vacancies, and therefore, the carrier concentration reduces. This can bring the degradation of the ON/OFF current ratio of the device. The ON/OFF ratio of the device will increase for a higher value of drain voltage.

The transfer characteristic of the FET was also captured after exposing it to different gases such as ammonia, formaldehyde, toluene, and acetone. Fig. 3(c) shows I_d versus V_g plot of the sensor in bare condition and after exposing it to ammonia of different concentrations. The device shows same type of transfer characteristics as seen earlier. The output current decreases with its exposure to gases. Upon exposure of ammonia, transfer of electrons take place from ammonia to rGO, reducing the number of majority carrier holes, and therefore, the effective drain current decreases. A similar behavior was exhibited upon exposing the sensor to formaldehyde, toluene, and acetone. The I_d versus V_g plot of the device in bare condition and in formaldehyde, toluene, and acetone vapors is shown in Fig. 3(d)–(f). In both the cases,

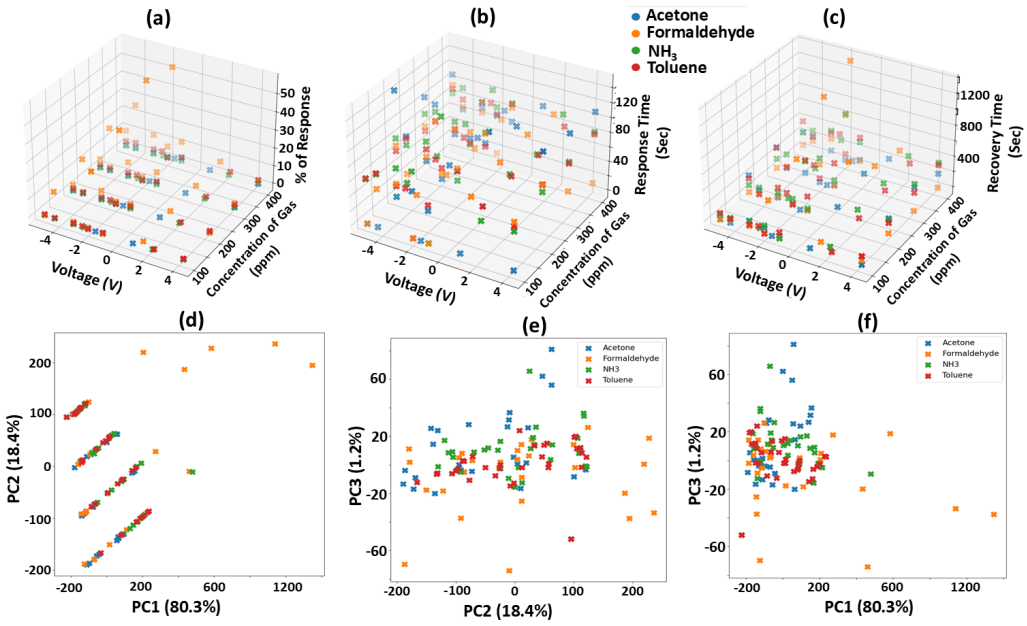

Fig. 6. Data distribution with respect to two independent parameters gate voltage and concentration of gas and one dependent parameter. (a) % of Response. (b) Response time. (c) Recovery time. (d)–(f) Data distribution after applying PCA.

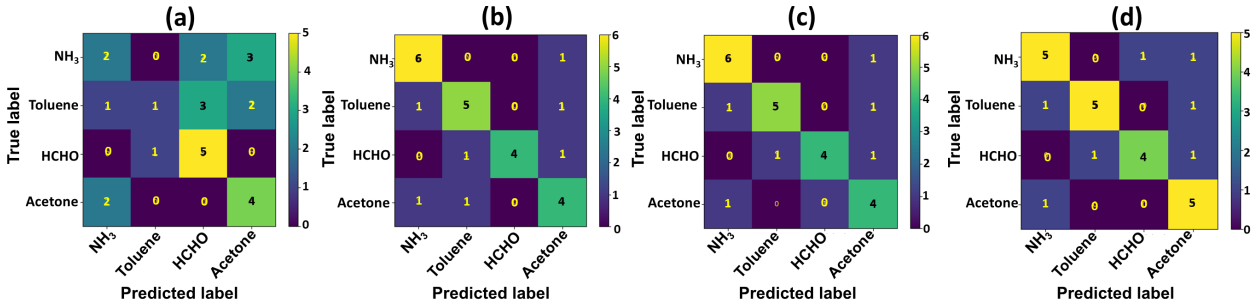

Fig. 7. Confusion matrix on the test dataset for (a) SVM, (b) DT, (c) GB, and (d) RF classifier.

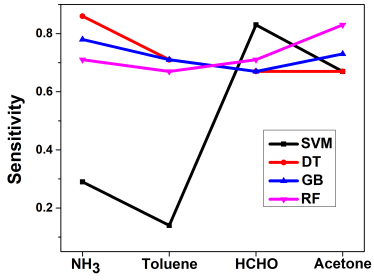

Fig. 8. Sensitivity plot for all four classifiers.

current decreases with gas exposure. On the other hand, a shift in threshold voltage was also noted upon exposure to gas. The threshold voltage can be determined by extrapolating the I_d to V_g intercept, and it is figured out that a negative shift in threshold voltage occurs when the device is exposed to all four gases.

Furthermore, the transient responses of the device were evaluated upon exposure to different concentrations of the above-mentioned gases (NH_3, HCHO, toluene, and acetone). The transient responses were captured at seven different gate voltages while keeping V_d fixed at 200 mV. Those responses of the device are delineated in Fig. 4 for three negative gate voltages. With exposure of gases, device current starts to fall. This phenomenon can be described in terms of adsorption and desorption of gas molecules in active sites of rGO. Electrons transfer take place from gas to rGO during adsorption, therefore decreasing the majority carrier hole through recombination. The consequences are an increment in channel resistances and reduction in overall device current. As soon as the gas flow is off, the active sites of rGO get occupied by the oxygen atoms and desorption of gas molecules occurs. As a result, electrons get removed from the sensing layer leaving the holes behind. Hence, the current increases and returns to its initial position. The device behaves in similar manner for all four gases. From transient responses, various features of the sensor, i.e., % of response, response time and recovery time are extracted. The % of response of the device was estimated for different gate voltages using

$$\text{Response} = \frac{R_{\text{air}} - R_{\text{HCHO}}}{R_{\text{air}}} * 100\%. \quad (1)$$

Fig. 5 shows the steady-state response of the sensor as a function of different gate voltages. The results indicate that sensor exhibited highest response at a particular gate voltage

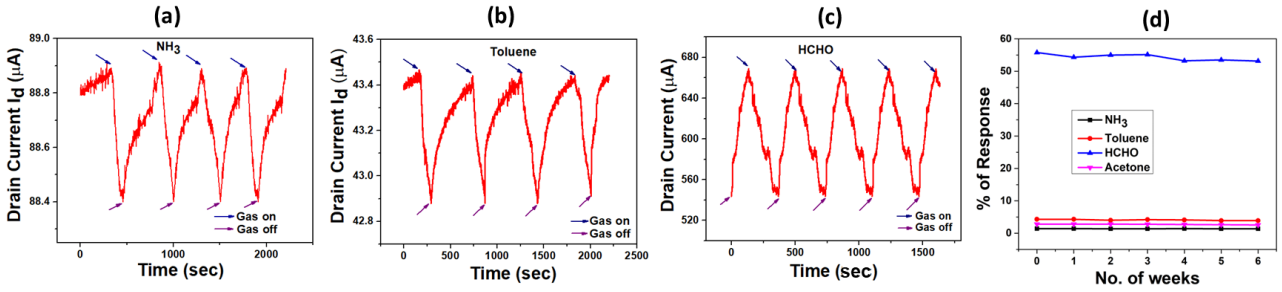

Fig. 9. Repeatability of the FET sensor upon exposure to 200 ppm (a) formaldehyde, (b) toluene, and (c) ammonia. (d) Stability test of the sensor.

of −2.3, −2.4, −1.7, and −1 V for ammonia, toluene, formaldehyde, and acetone, respectively. The response of the device becomes maximum when the number of holes in the channel is such that the fraction of holes lost is maximum due to the contribution of electrons from gases. If the gate voltage is further increased, the number of holes reduces, reducing interaction probability with the incoming electrons. However, a further decrease in gate voltage leads to more holes in the channel. Even though the interaction probability increases, the fraction of holes lost during sensing reduces, degrading the sensor device's response.

C. Data Processing Using Machine Learning Algorithms

Following the gas sensing measurements, we extracted relevant features from the response profiles of each of the four gases. The features such as the percentage of response, response time, and recovery time of each gas at different concentrations were considered. Unlike other research [13], [23], we did not further process these features for our classification task. For example, Kanaparthi and Singh [13] used a ternary logic based on the response profiles of gases. However, in our case, all the gases generate the same ternary logic features. Conversely, Huang et al. [23] used exponential functions and fit the exposure and flushing phases of the response profiles to obtain a total of 11 features. However, we used only the magnitude of extracted features (% of response, response time, and recovery time) in our machine learning analysis. A total of 32 features were recorded for each gas, which produced 128 features for four gases. We visualized our data points with respect to two independent parameters, such as gate voltage and gas concentration, and three dependent parameters, respectively, in Fig. 6. It is clear that the gases are not clearly differentiable other than formaldehyde, which is perceptually separated in Fig. 6(a).

Therefore, principal component analysis (PCA) was applied to analyze our dataset. The PCA is a nonparametric statistical technique primarily used for dimensionality reduction of the data with the aim of maintaining most of the relevant information. The first principal component explains 80.3% of the variance, while the second and third components explain 18.4% and 1.2% of the variance, respectively. We did not consider the last two components as they did not represent any information related to the data. The PCA score plots of our dataset are presented in Fig. 6(d)–(f). Here also, the data points of formaldehyde gas are clearly distinguishable from other gases. It is obvious that given the type of device we used, the formaldehyde gas will be clearly detected. However, we want to distinguish other gases also, for which we explored four different classification mechanisms.

Four different classification mechanisms, such as SVM, DT, GB, and RF, were explored to analyze the sensor's capability to distinguish all four gases. We used our 128 data points corresponding to the four gases to train each classification model. All the feature values were first normalized with zero mean and unit variance. This reduces the bias and inconsistency of the trained model and also improves its stability. The whole dataset was then divided into the training and evaluation set in an 80:20 ratio with scuffling, to investigate the prediction accuracy of each classifier. The fivefold hold-one-out cross-validation was used during the training of each classifier to ensure better generalization. It also reduced the chance of overfitting during training. Fig. 7 shows the confusion matrix achieved by all four classifiers on our test data. Other than SVM, all three classifiers achieved an accuracy of 73% on the test data. However, SVM only classified the formaldehyde data properly with a sensitivity value of 0.83 and poorly classified all other gases. The sensitivity plot for all four classifiers is illustrated in Fig. 8. It can be argued that all three classifiers other than the SVM recognize each gas with a similar sensitivity, which also proves the classifier's generalization. Our result also indicates that the model cannot differentiate all gases with high accuracy due to the generation of almost similar feature values for all three gases except formaldehyde (shown in Fig. 6). A curation of data may be required to achieve higher accuracy of classification models, which will be done as part of future work.

D. Repeatability and Stability Testing

Finally, the reliability of the FET sensor was evaluated through repeatability and stability testing. Fig. 9(a)–(c) shows the repeatability curves of the device toward 200 PPM formaldehyde, toluene, and ammonia vapors, respectively. Repeatability testing in formaldehyde, toluene, and ammonia vapors was carried out at $V_g = -1.7$, -2.4, and -2.3 V, respectively where highest response was achieved. From the result, it is seen that the variation in response for multiple cycles is minimum. The sensor was put to a stability test for six-week duration against 400 PPM concentration of each gas. Fig. 9(d) depicts the same stability plot where it is observed that the response is stable over time.

From the results of all the experiments listed above, it can be deduced that the proposed method is effective for the detection of four gases including ammonia, toluene, formaldehyde, and acetone using a single FET sensor.

IV. Conclusion

In summary, this article presents a method for the automated prediction of target gases with a single FET-based gas sensor through gate voltage sweeping and machine learning algorithms. The sensing material, i.e., L-ascorbic acid reduced rGO behaved like a p-type semiconducting material and forming the channel of the FET sensor. Various features of the sensor were recorded as a function of gate voltages and concentration after exposing it to different target gases. Later, those extracted features were used for gas prediction. A list of classification methods, such as DT, SVM, GB, and RF, were adopted to train the prediction model using the extracted features to detect the gas. Among them, DT, GB, and RF achieved the highest accuracy of 73% for our dataset. We also saw that each classification model could generalize our data properly despite using raw response profiles and considering its complexities.

As per the author's knowledge, this is the first time a gate-tuned sensor has been developed that can discriminate four gases at different gate voltages, when an unknown gas among the four is exposed to the sensor. The sensor behaves differently at different gate voltages. Therefore, several sensors in a sensor array can be replaced by one single sensor (behaving like several sensors at different gate voltages) and analyzed at different gate voltages. Furthermore, the sensor also exhibits high sensitivity, repeatability, and stability.

References

[1] S. Tripathy, A. Sett, S. Majumder, and T. K. Bhattacharyya, "Study of gate induced sensitivity amplification in carbon nanotube thin film transistor based ammonia sensor," *Sens. Actuators B, Chem.*, vol. 382, May 2023, Art. no. 133511.

[2] S. Kanaparthi and S. G. Singh, "Chemiresistive sensor based on zinc oxide nanoflakes for CO_2 detection," *ACS Appl. Nano Mater.*, vol. 2, no. 2, pp. 700–706, Feb. 2019.

[3] S. Kanaparthi and S. G. Singh, "Drift independent discrimination of H_2S from other interfering gases with a metal oxide gas sensor using extracted adsorption-desorption noise," *Sens. Actuators B, Chem.*, vol. 344, Oct. 2021, Art. no. 130146.

[4] A. Blanco-Rodríguez et al., "Development of an electronic nose to characterize odours emitted from different stages in a wastewater treatment plant," *Water Res.*, vol. 134, pp. 92–100, May 2018.

[5] Z. Yuan et al., "Trace-level, multi-gas detection for food quality assessment based on decorated silicon transistor arrays," *Adv. Mater.*, vol. 32, no. 21, May 2020, Art. no. 1908385.

[6] A. Sett, L. Sarkar, and T. K. Bhattacharyya, "Amplification of arsenic sensitivity in functionalized zinc oxide field effect transistor through optimization of gate electrostatics," *Appl. Phys. Lett.*, vol. 121, no. 20, Nov. 2022, Art. no. 203509.

[7] A. Sett, L. Sarkar, S. Majumder, and T. K. Bhattacharyya, "Amplification of ammonia sensing performance through gate induced carrier modulation in Cur-rGO silk-FET," *Sci. Rep.*, vol. 13, no. 1, p. 8159, May 2023.

[8] J. H. An and J. Jang, "A highly sensitive FET-type aptasensor using flower-like MoS_2 nanospheres for real-time detection of arsenic(iii)," *Nanoscale*, vol. 9, no. 22, pp. 7483–7492, 2017.

[9] G. Zhou, H. Pu, J. Chang, X. Sui, S. Mao, and J. Chen, "Real-time electronic sensor based on black phosphorus/Au NPs/DTT hybrid structure: Application in arsenic detection," *Sens. Actuators B, Chem.*, vol. 257, pp. 214–219, Mar. 2018.

[10] N. Shehada, G. Brönstrup, K. Funka, S. Christiansen, M. Leja, and H. Haick, "Ultrasensitive silicon nanowire for real-world gas sensing: Noninvasive diagnosis of cancer from breath volatolome," *Nano Lett.*, vol. 15, no. 2, pp. 1288–1295, Feb. 2015.

[11] F. Gu, C. Li, D. Han, and Z. Wang, "Manipulating the defect structure (V_O) of In_2O_3 nanoparticles for enhancement of formaldehyde detection," *ACS Appl. Mater. Interfaces*, vol. 10, no. 1, pp. 933–942, 2018.

[12] C. Xie, L. Xiao, M. Hu, Z. Bai, X. Xia, and D. Zeng, "Fabrication and formaldehyde gas-sensing property of ZnO–MnO_2 coplanar gas sensor arrays," *Sens. Actuators B, Chem.*, vol. 145, no. 1, pp. 457–463, Mar. 2010.

[13] S. Kanaparthi and S. G. Singh, "Discrimination of gases with a single chemiresistive multi-gas sensor using temperature sweeping and machine learning," *Sens. Actuators B, Chem.*, vol. 348, Dec. 2021, Art. no. 130725.

[14] E. C. Nallon, V. P. Schnee, C. J. Bright, M. P. Polcha, and Q. Li, "Discrimination enhancement with transient feature analysis of a graphene chemical sensor," *Anal. Chem.*, vol. 88, no. 2, pp. 1401–1406, Jan. 2016.

[15] S. Rumyantsev, G. Liu, M. S. Shur, R. A. Potyrailo, and A. A. Balandin, "Selective gas sensing with a single pristine graphene transistor," *Nano Lett.*, vol. 12, no. 5, pp. 2294–2298, May 2012.

[16] A. Sett and T. K. Bhattacharyya, "Functionalized gold nanoparticles decorated reduced graphene oxide sheets for efficient detection of mercury," *IEEE Sensors J.*, vol. 20, no. 11, pp. 5712–5719, Jun. 2020.

[17] L. Sarkar, A. Sett, S. Majumdar, and T. K. Bhattacharyya, "Reduced graphene-oxide-based silk-FET: A facile platform for low power and room temperature detection of formaldehyde," *IEEE Trans. Electron Devices*, vol. 70, no. 6, pp. 3275–3281, Jun. 2023.

[18] L. Sarkar, B. P. Yelagala, S. G. Singh, and S. R. K. Vanjari, "Electrodeposition as a facile way for the preparation of piezoelectric ultrathin silk film–based flexible nanogenerators," *Int. J. Energy Res.*, vol. 46, no. 3, pp. 3443–3457, Mar. 2022.

[19] G. Jiang et al., "Free-standing functionalized graphene oxide solid electrolytes in electrochemical gas sensors," *Adv. Funct. Mater.*, vol. 26, no. 11, pp. 1729–1736, Mar. 2016.

[20] A. Sett, S. Majumder, and T. K. Bhattacharyya, "Flexible room temperature ammonia gas sensor based on low-temperature tuning of functional groups in grapheme," *IEEE Trans. Electron Devices*, vol. 68, no. 7, pp. 3181–3188, Jul. 2021.

[21] X. Mei and J. Ouyang, "Ultrasonication-assisted ultrafast reduction of graphene oxide by zinc powder at room temperature," *Carbon*, vol. 49, no. 15, pp. 5389–5397, 2011.

[22] S. Azizighannad and S. Mitra, "Stepwise reduction of graphene oxide (GO) and its effects on chemical and colloidal properties," *Sci. Rep.*, vol. 8, no. 1, pp. 1–8, 2018.

[23] S. Huang et al., "Machine learning-enabled smart gas sensing platform for identification of industrial gases," *Adv. Intell. Syst.*, vol. 4, no. 4, Apr. 2022, Art. no. 2200016.